Transitions between multiple dynamical states in a confined dense active-particle system

Pallab Sinha Mahapatra
Department of Mechanical Engineering, Indian Institute of Technology Madras, Chennai 600036, India

Ajinkya Kulkarni, Sam Mathew, and Mahesh V. Panchagnula
Department of Applied Mechanics, Indian Institute of Technology Madras, Chennai 600036, India

Srikanth Vedantam
Department of Engineering Design, Indian Institute of Technology Madras, Chennai 600036, India
(Received 5 January 2017; published 28 June 2017)

We study the collective motion of a dense suspension of active swimmers in a viscous fluid medium. The swimmers are modeled as soft spheres moving in a highly viscous fluid medium. The magnitude of the propelling thrust exerted by each particle is taken to be a constant and the direction is aligned to its velocity. Depending on the magnitude of the exerted thrust, several nonequilibrium steady states are observed. The transitions between the steady states are characterized using the total dissipation as a function of the magnitude of the thrust. The transitions between the nonequilibrium states are characterized by changes in exponent at low thrust values. At high thrust values, hysteretic transitions between ordered and disordered states are observed.

DOI: 10.1103/PhysRevE.95.062610

I. INTRODUCTION

The mechanics of matter composed of individual independently moving particles is quite complex. Among such granular materials, distinction can be made between passive particles which are propelled by external forces and active particles which are able to self-propel. Swarms of such self-propelling objects moving collectively display very interesting dynamics as observed in schools of fishes or flocks of birds [1]. This collective behavior is observed in a range of length scales spanning micoorganisms to human crowds. At small length scales, bacterial colonies [2] and sperm cells [3] show interesting patterns of motion. Examples of collective behavior at larger length scales include human crowds [4], active granular media [5], polar active particles [6], and colloidal particles [7]. Recent advances in the field of active matter can be found in several seminal works [8–11].

Even in self-propelling active matter, the organized collective motion arises from two reasons: (1) Individual particles are able to observe neighbors and adjust the direction of motion, and (2) hydrodynamic effects of the surrounding medium could provide the coupling. In general, the effects of these two mechanisms may not be equivalent and a combination could contribute to the collective motion. We are interested in the latter case where hydrodynamic interactions are thought to help reduce the total energy expenditure of the particles by minimizing viscous dissipation. Hydrodynamic interactions are important in the motion of bacteria and other microorganisms using beating of flagella or cilia [12] in a viscous medium at low-Reynolds-number swimmers and is of interest in potential technological applications.

Models of these phenomena have generally been of two types: (a) continuum models obtained by considering field of orientation vectors representing particles coupled to standard hydrodynamics equations and (b) discrete particle models. Toner and Tu [13] proposed a nonequilibrium continuum dynamical model for the collective motion of the biological organisms. The most common particle-based model without any hydrodynamic interactions has been the Vicsek model (VM) [14] and its variants. In this model, the particles are assumed to interact with their neighbors within a certain distance and align themselves in the average direction of the velocities of the neighbors. This method works well for low-noise and high-particle-density systems [15]. Lu *et al.* [16] used an improved self-propelled model for identifying the transition from a collective state to random motion of bacteria. Laskar *et al.* [17] described the spontaneous motion of active filaments in three dimensions by considering a minimal active filament model with the hydrodynamic interaction. Baskaran and Marchetti [12] showed that large-scale nonequilibrium phenomena can be observed due to hydrodynamic interactions between the active particles. Collective behavior has also been observed without having any alignment mechanism in the self-propelled suspension [18].

Experiments as well as theoretical studies confirm the presence of different kinds of global patterns of the self-propelled systems. Tsang and Kanso [19] reported that geometric confinement and flagellar activity of microswimmers result in hydrodynamically triggered phase transitions. They identified three phases: chaotic swirling, stable circulation, and boundary aggregation. Transitions between phases in dense active colloids [7] or soft active particles [20] inside a box has been observed. Depending on the packing fraction (or density) solid or gaslike phases and sometimes cluster [7] phases have been identified. In the high viscous regime, different low-energy states of the self-propelled particles, namely the coherent flock, the rigid rotation, and the random droplet have been identified [21]. Solon *et al.* [22] demonstrated the microphase separation using Viscek model in the coexistence region.

In most earlier work, the fluid medium is either ignored and the collective motion is obtained from neighboring particle heuristics or the hydrodynamics interactions are modeled in detail through a solution of Navier-Stokes equations in the appropriate regime. In this work, we account for the

hydrodynamic interactions through Stokes drag, thus obviating the need for explicit solution of the hydrodynamic equations. Our model is a generalization of our earlier work on wet granular slurries [23,24] and is valid in the regime of viscosity-dominated low-inertia fluid medium. Under this assumption, the fluid velocity at a point is obtained by an average velocity of particles in a neighborhood of the point. The thrust is taken to be oriented in the instantaneous direction of the particle velocity and of constant value. We study the behavior of a dense collection of self-propelled particles in a square cavity.

In order to characterize equilibrium thermal phase transitions, a physical quantity such as the specific free energy is studied in terms of the reduced temperature and the changes in power law exponents across the transition. In analogy, we consider the total dissipation as a function of the thrust to characterize the transitions between the dynamical states in this problem.

We begin with first describing the model and the numerical approach. Next, we present results of simulations in which the thrust is increased gradually over a wide range. We observe characteristic steady states for ranges of the thrust values. These transitions are characterized by the total dissipation in the system. Both continuous and hysteretic transitions are observed in this model.

II. MODEL

A. Governing equations

Our model is based on that of a wet granular slurry presented earlier [23,24]. The particles are taken to be immersed in a viscous liquid and all particles are able to propel themselves. We consider a fixed number of N interacting spherical particles of equal radius r and mass m, constrained to move within a frictionless two-dimensional square cavity. The particles are modeled as soft disks of finite mass. The fluid inertia in this model is taken to be small in comparison to the particle inertia.

The total force on the ith particle $\vec{F}_i$ is taken to be the sum of an interparticle force $\vec{F}_{pp,i}$, self-propelled force $\vec{F}_{sp,i}$, and dissipative force $\vec{F}_{d,i}$,

$$\vec{F}_i = \vec{F}_{pp,i} + \vec{F}_{sp,i} + \vec{F}_{d,i}. \tag{1}$$

Following Refs. [23,24], the interparticle interaction force $\vec{F}_{pp,i}$ is taken to be of a linear soft-sphere form

$$\vec{F}_{pp,i} = \begin{cases} -k_n\vec{\delta}, & |\vec{\delta}| > 0 \\ \vec{0}, & \text{otherwise,} \end{cases} \tag{2}$$

where $\vec{\delta} = \{|\vec{r}_i - \vec{r}_j| - [(d_i + d_j)/2]\}\frac{\vec{r}_i - \vec{r}_j}{|\vec{r}_i - \vec{r}_j|}$ is the separation of two particles i and j in terms of position vectors $\vec{r}_i$ and $\vec{r}_j$ and diameters d_i and d_j for all neighboring particles j. The direction of the force is along the line joining the particle centers.

The self-propelled force $\vec{F}_{sp,i}$ is modeled as

$$\vec{F}_{sp,i} = m_i(\beta - \alpha|\vec{v}_{p,i}|^2)\hat{v}_{p,i}, \tag{3}$$

where m_i is the mass of the particle, $\hat{v}_{p,i}$ is a unit vector in the direction of the velocity of the ith particle $\vec{v}_{p,i}$, and β is a thrust coefficient. α is a small positive coefficient introduced to ensure that a single particle in a dilute suspension does not exhibit unbounded acceleration [25]. One can also rationalize α as a net momentum sink since the thrust itself is being modeled as a monopole force. For dense ensembles, this issue does not arise. α can even be set to zero in such a case without loss of generality. This was the choice exercised in this case.

The dissipative force on each particle arising from the surrounding fluid medium is estimated using Stokes' drag. The equation for the dissipative coordination force on the ith particle is taken to be proportional to the relative velocity between a particle and the fluid at that location [24],

$$\vec{F}_{d,i} = C_v d_i(\vec{v}_i - \vec{v}_{p,i}), \tag{4}$$

where C_v is a coordination coefficient analogous to the Stokes' drag coefficient $3\pi\mu$ with μ the fluid viscosity. C_v is a measure of the local coordination each particle experiences with its neighbors. $\vec{v}_i$ is the velocity of the fluid determined from a weighted mean of the surrounding particles. The relative velocity is determined based on n neighboring particles surrounding the ith particle [24]:

$$\vec{v}_i = \frac{\sum_{j=1}^{n} m_j W_{ij}(\|\vec{r}_i - \vec{r}_j\|, h_i)\vec{v}_j}{\sum_{j=1}^{n} m_j W_{ij}(\|\vec{r}_i - \vec{r}_j\|, h_i)}, \tag{5}$$

where the weighing function W_{ij} is of a Gaussian form given by

$$W_{ij} = \begin{cases} \exp\left(-\eta\frac{\|\vec{r}_i - \vec{r}_j\|^2}{{h_i}^2}\right), & \frac{\|\vec{r}_i - \vec{r}_j\|}{h_i} \leqslant 1, \\ 0, & \text{otherwise,} \end{cases} \tag{6}$$

and h_i is a radius of influence for particle i which corresponds to the extent to which the particle's neighborhood influences the fluid velocity. η is taken as 2 in our simulations following Drumm *et al.* [26]. Consistent with the assumption that fluid inertia is small in comparison to particle inertia, the calculated fluid velocity $\vec{v}_i$ is taken to be zero if there are no surrounding particles in the neighborhood.

Our model of the fluid drag follows from our previous work [23,24], where each particle experiences a drag due to the relative velocity between the fluid and its own motion. The fluid velocity is estimated using a weighted average of velocities of the surrounding particles. Through this approach, we are able to estimate the fluid velocity field without needing to explicitly solve the Navier-Stokes equations in a coupled framework. We have shown in our previous work [23,24] that this approach is valid for studying the dynamics of dense suspensions. As can be seen from Eq. (4), the effect of the fluid is through a hydrodynamic drag on the particles. This drag force penalizes absence of local coordination and therefore gives rise to coordinated motion. In the absence of the fluid (or this force), only thermal motion will be observed.

B. Simulation details

We perform the simulations in a two-dimensional square domain. Disks of 5 mm diameter are initially packed at 74% area fraction in a square lattice. The domain is filled with 6084 particles. The walls of the domain are modeled as fixed disks of the same size as the particles.

The acceleration of each particle is given by the algebraic sum of the forces on each particle divided by its mass. The acceleration is integrated numerically to position and velocity

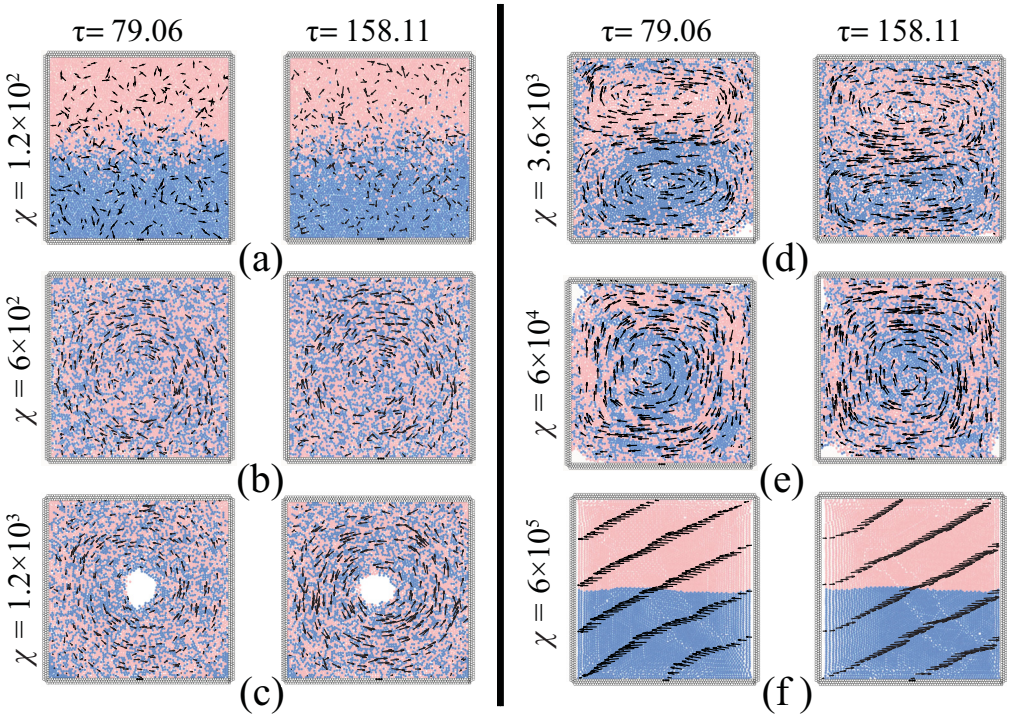

FIG. 1. Steady phases at different χ are shown at two different values of nondimensionalized time $\tau = t/\sqrt{\frac{L}{\beta}}$. Representative velocity vectors are overlaid (the black arrows) with the particles to show the overall motion at each phase. (a) Random motion of particles at $\chi = 1.2 \times 10^2$. (b) Circular motion at $\chi = 6 \times 10^2$. (c) Circular motion of particles at $\chi = 1.2 \times 10^3$ with a particle-free inner core region. (d) Two circulating cells state at $\chi = 3.6 \times 10^3$. (e) Rotary motion with self-sustaining vortices are observed for $\chi = 6 \times 10^4$. (f) Oscillatory motion spanning the whole domain is shown for $\chi = 6 \times 10^5$.

as a function of time using the velocity Verlet algorithm [27]. More details about the algorithm is given in our earlier work [24]. Accurate determination of forces on each time step is computationally very expensive; a linked list algorithm is therefore used to reduce the computational effort [28].

III. RESULTS AND DISCUSSION

The dynamics of this system is governed by three dimensionless groups: $\bar{L} = \frac{L}{d}$, $\bar{k} = \frac{k_n d}{m\beta}$, and χ. The definition of χ arises as a ratio of two force scales. F_d is a local hydrodynamic coordination force (due to drag), where $F_d \sim C_v d\sqrt{\beta \bar{L}}$. Here $\sqrt{\beta \bar{L}}$ is a scale associated with the maximum possible speed in the domain. The second force scale is the thrust given by $F_p \sim m\beta$. A ratio of these two scales will yield $\chi = \bar{L}\frac{F_d}{F_p}$. On simplification, one can define

$$\chi = \frac{C_v L\sqrt{L}}{m\sqrt{\beta}}. \tag{7}$$

We have discussed the effect of χ on the phase transition characteristics, since it conceptualizes the competition between the hydrodynamic and propulsion forces. We have varied χ by changing C_v while maintaining β and the other parameters constant. As long as one varies χ while keeping $\bar{L}$ and $\bar{k}$ the same, one will obtain the same results. At low χ or C_v, the thrust force is high relative to the drag force. We note that, in this model, the dissipative force promotes the alignment of the particles. This is because the drag force on a particle is proportional to the *relative velocity* of the particle and the fluid medium at that point. If the particle velocity is the same as that of the fluid medium, the drag force is zero. The velocity of the fluid at the location of the particle is the weighted average of the surrounding particles. Thus the drag force promotes the alignment of the particle velocity with the neighbors. The drag coefficient C_v plays the key role in determining the magnitude of the drag force.

We begin the simulations with $\chi = 60$. For aiding visualization, the particles are colored blue and pink depending on their initial position. Particles initially in the top half are colored pink and those in the bottom half of the cavity are colored blue. We increase χ in steps of 6 allowing for sufficient time at each value of χ for the system to attain a steady state. For different ranges of χ, we observe various steady states as shown in Fig. 1. The two columns for each value of χ show the system at two time instants in order to obtain a sense of the steady-state configurations attained by the system. All different phases are shown in the Supplemental Material [29].

At low values of $\chi = 1.2 \times 10^2$, we have random trajectories of the particles akin to thermal noise as shown in Fig. 1(a). Low values of χ correspond to a reduced tendency of the particle to coordinate with its immediate neighbors, as discussed earlier. As χ is increased gradually in steps of 6, we observe a sharp transition towards an organized vortical state at $\chi = 3.36 \times 10^2$. For values of χ between 1.2×10^2 and 3.36×10^2, the particles move in random trajectories spanning the domain. The random motion of the particles is due to the dominance of particle-particle collisions and the

thrust force in relation to the drag force. Diffusion of the particles can be observed at the interface between the blue and pink particles. For the range $3.36 \times 10^2 \leqslant \chi \leqslant 6.72 \times 10^2$, we observe collective behavior of the particles in the form of periodic rotary motion as shown in Fig. 1(b). In this regime, the particles travel around the center of the cavity. Since the χ for this regime is still low, this state is not immediately attained. This state is only observed upon performing the simulation for a sufficiently long time.

At higher values of χ in the range $6.78 \times 10^2 \leqslant \chi \leqslant 3 \times 10^3$, a central particle-free void is observed, as can be seen in Fig. 1(c). It is observed that for a fixed χ, the location and the size of the core remains fairly invariant with respect to time. As shown in the Supplemental Material [29], this regime also displays characteristics of slow diffusion in the radial direction. The formation of the central core is a result of higher rotational speeds at which the centrifugal forces aid formation of this particle-free region.

For $3.24 \times 10^3 \leqslant \chi \leqslant 4.2 \times 10^3$, two rotating cells form and rotate about their own centers as shown in Fig. 1(d). This state is observed to be metastable in the sense that the two cells break down to a single cell and reform over different time intervals.

Next, a rotary motion with an oscillating unfilled core is observed for higher values of $\chi > 4.2 \times 10^3$. A sample case for $\chi = 6 \times 10^4$ is shown in Fig. 1(e). The values of average speed of a single agent are low in this regime and become smaller with increasing χ. In to contrast the case shown in Fig. 1(b), segregation of the blue and pink particles can be observed. This is due to the fact that the particles begin the rotational motion from their initial state and diffusion is relatively small.

For very high values of $\chi > 1.56 \times 10^3$, we observe an interesting state, where all particles oscillate together horizontally like a viscous fluid with no bulk motion of the particles [29]. A sample case for $\chi = 6 \times 10^5$ is shown in Fig. 1(f). We have identified different states and transitions between them, depending on the relative magnitudes of the thrust and dissipative forces. Some of the states identified by us have been observed by Seyed-Allaei and Ejtehadi [30], which they term homogeneous gaseous phase, band structures, moving clumps, moving clusters, vibrating rings, and vortical structures, by using a combined continuous Vicsek model and repulsive particle system model. Similar observations have been reported in Ref. [31] as well.

We characterize the states and transitions between them quantitatively using the total energy dissipation. With increasing χ, the velocities of the individual particles decreases and thus the total dissipation decreases. The viscous dissipation at a point in the domain is calculated using

$$\phi = 2\mu\left\{\left(\frac{dv_x}{dx}\right)^2 + \left(\frac{dv_y}{dy}\right)^2\right\} + \mu\left(\frac{dv_y}{dx} + \frac{dv_x}{dy}\right)^2. \quad (8)$$

Here, v_x and v_y are the local velocity field components of the particles at a particular location. It should be noted that, for the sake of simplicity, we have not considered the change of the shape of the individual particle. Let us define a total free energy dissipated during the time interval $0 \leqslant t \leqslant T$ as $\phi^T = \int_0^T \int_{\forall} \phi d\forall dt$. Here, $\forall$ is the total volume of the domain and T is a long enough time to ensure a stable average. From this, the nondimensional version of ϕ^T, called Φ, can be defined as

$$\Phi = \frac{\phi^T}{C_v L^2 \sqrt{\beta L}}, \quad (9)$$

using the scales defined earlier. It must be mentioned that Φ is an estimate of total energy dissipated by the system, which is proportional to the total entropy produced in the same time interval. According to the general extremal principle, it can be used as a predictor of steady states [21].

In Fig. 2 the variation of the magnitude of the total dissipation is shown with the dimensionless number χ. Here, we have increased χ from 60 to 6×10^5 by keeping the same initial conditions of all the simulations. Transitions between the different steady states are observed due to an increase of χ. As discussed earlier and also can be seen from Fig. 2, there are mainly three phases: thermal motion, rotation, and oscillation. Therefore, from Fig. 2, it can be said that with increase of χ, total dissipation of the system decreases and the behavior of the particles changes from thermal motion ($\chi \leqslant 3.36 \times 10^2$) to the oscillatory state ($\chi > 6 \times 10^5$). The thrust forces add power to the system at each time step, leading to a oscillatory state from the regime of random motion. The sharp transition from the thermal motion to rotation is shown in the insets of Fig. 2. The time-averaged velocity vectors show the sharp transition from the thermal motion to rotation phase at $\chi = 332.15$. A continuous decrease in Φ was observed for transitions B and C.

Finally, we perform simulations with increasing χ from 60 to 6×10^5 and then gradually reducing χ back to 60. The total dissipation is plotted against χ as shown in Fig. 3. The total dissipation with increasing χ is shown using a red line and the decreasing χ is shown in black. Two sets of simulations were performed to investigate the nature of the transitions. In the first case, we have increased the value of χ from 60 to 6×10^5. Each simulation was performed for a time long enough ($\tau > 600$) to reach a steady state. The next simulation was started by taking the final state of the particles of the previous χ as initial condition with an increase of χ value of 6. A similar procedure was followed by lowering the χ values from 6×10^5 to 60 with a step of 6. In the regions of low χ, we observe random motion of the particles—the thermal motion phase. Two distinct hysteretic zones were identified from Fig. 3. During the random motion of the particles, at low χ values, a hysteretic characteristic is observed with a higher value of dissipation during the decreasing χ. We have identified two routes of phase transitions depending on the initial condition. As shown in Fig. 2, when all the simulations were started with the same initial condition, the transition from the one vortex motion to the thermal motion is continuous. On the other hand, when simulations were started by taking the final state of the previous simulation as the initial condition, a delayed transition was observed (see Fig. 3). The hysteretic transition between thermal and rotary phases occurs due to a competition between a particle's own motivation to retain its thrust direction and the neighborhood's hydrodynamic influence to cause a change. Similar hysteretic phase transition has also been reported by Solon *et al.* [22], where the effect of the neighborhood particles is decreased due to a decrease in the density. Conceptually,

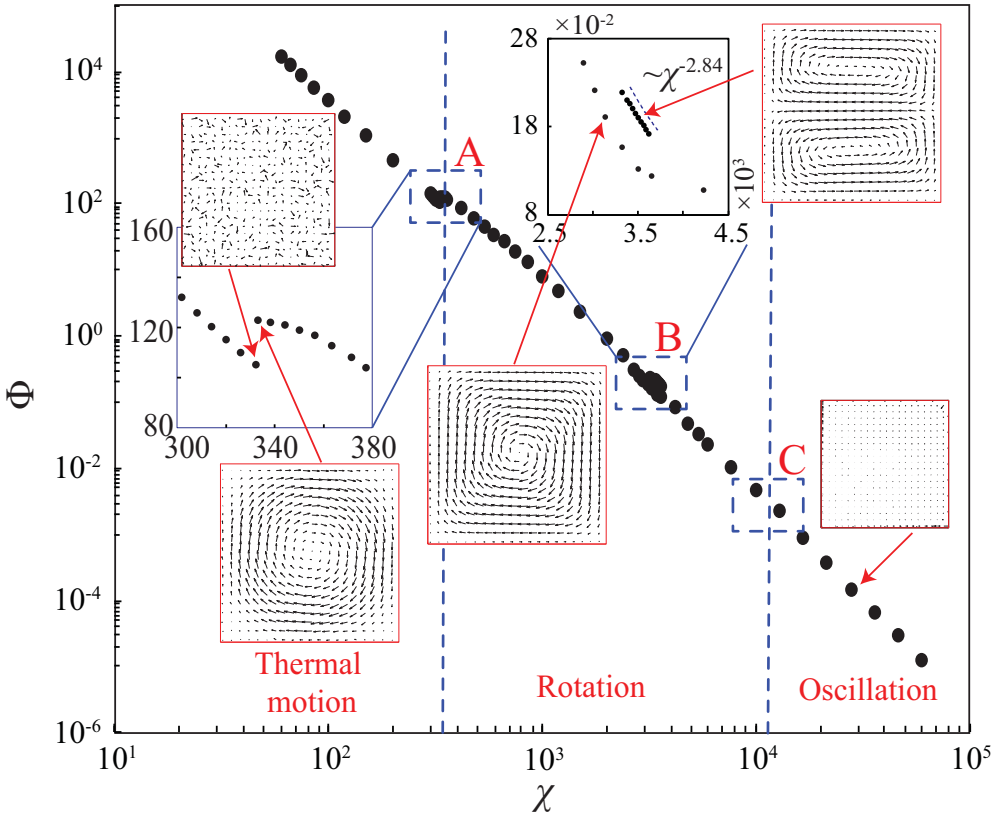

FIG. 2. Total dissipation with the nondimensional group χ is shown. Phase transitions with the different χ values are observed. Total dissipation Φ decreases with an increase of χ. Three distinct phases are observed: thermal motion, rotation, and oscillation. Two separate phase transitions are shown: (A) thermal motion to rotation and (C) rotation to oscillation; the presence of a metastable phases of double vortex and single vortex is shown in panel (B). Time-averaged velocity vectors are shown in the insets for different phases.

these two routes to hysteretic transitions are governed by similar physics.

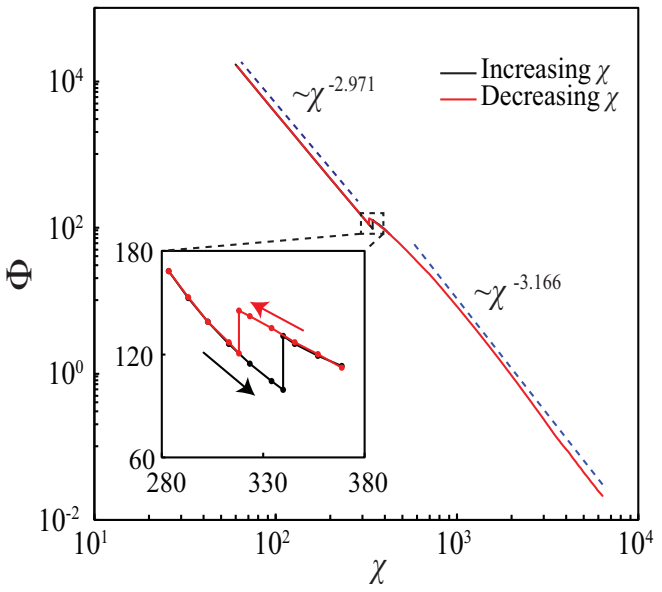

FIG. 3. The total dissipation with increasing χ is shown using a red line and decreasing χ is shown in black. Hysteresis due to an increase or decrease of χ values is observed near the transition from thermal motion to rotation.

It is interesting to note from Fig. 3 that far from the critical transition points, $\Phi \sim \chi^{-3}$. This scaling appears to hold both in the thermal motion regime as well as in the rotary state regime. This implies that

$$\frac{\phi^T}{C_v L^2\sqrt{\beta L}} \sim \left(\frac{C_v L\sqrt{L}}{m\sqrt{\beta}}\right)^{-3}. \tag{10}$$

A comparison of the hydrodynamic force and self-propelled force acting on a single particle (of diameter d and mass m) can be written as

$$C_v|\vec{v}_i - \vec{v}_{p,i}|d \sim m\beta. \tag{11}$$

By simplifying this equation, one obtains the following scaling for the slip velocity between the particle velocity and the fluid velocity

$$|\vec{v}_i - \vec{v}_{p,i}| \sim \frac{m\beta}{dC_v}. \tag{12}$$

Recasting the Eq. (10) using Eq. (12), one obtains

$$\phi^T \sim m\left(\frac{d}{L}\right)^2\left(\frac{m\beta}{dC_v}\right)^2. \tag{13}$$

Using Eq. (12), one can write $\phi^T \sim c|\vec{v}_i - \vec{v}_{p,i}|^2$, where c is a proportionality constant. This suggests that the drag force on a single particle in a dense suspension is of the Stokes form, where the energy dissipation is proportional to the square of the slip velocity.

We have observed a transition from thermal motion to a fluidic state (rotary phase) due to an increase of χ. This transition bears a striking resemblance to the glass-fluid phase transition observed by previous researchers [32–37]. The glassy phase was observed when the density of the particles is greater than the glass transition density [32]. In the present work, the collection of particles behaves like a fluid when the exerted thrust by each particle is low (at higher χ). At higher thrust, the particles are trapped in a high configurational entropy state where the behavior is reminiscent of a glass.

IV. CONCLUSION

We have systematically studied various steady states of an active particle system. Our model uses a Stokes approach to treat hydrodynamic interactions, which play the key role in the collective motion of the particles. We characterize the steady states and their transitions by the total dissipation which appears to be a natural way of characterizing nonequilibrium systems. Hysteresis is present in transitions between a gaseous state (thermal motion) and a rotational state. We have also observed a two-vortex metastable solution in a certain range of χ, which sharply transitions to the single vortex rotational state at two critical values of χ. Finally, we have also observed that away from these critical transition points, $\Phi \sim \chi^{-3}$ in the four dynamical states—thermal, single- and two-vortex rotational, as well as in the oscillatory states.

ACKNOWLEDGMENTS

The authors are thankful to the Indian Institute of Technology Madras computational resources in the High Performance Cluster for carrying out this work.

[1] I. D. Couzin, J. Krause, R. James, G. D. Ruxton, and N. R. Franks, Collective memory and spatial sorting in animal groups, J. Theor. Biol. **218**, 1 (2002).

[2] C. Dombrowski, L. Cisneros, S. Chatkaew, R. E. Goldstein, and J. O. Kessler, Self-Concentration and Large-Scale Coherence in Bacterial Dynamics, Phys. Rev. Lett. **93**, 098103 (2004).

[3] I. H. Riedel, K. Kruse, and J. Howard, A self-organized vortex array of hydrodynamically entrained sperm cells, Science **309**, 300 (2005).

[4] J. L. Silverberg, M. Bierbaum, J. P. Sethna, and I. Cohen, Collective Motion of Humans in Mosh and Circle Pits at Heavy Metal Concerts, Phys. Rev. Lett. **110**, 228701 (2013).

[5] J. Deseigne, O. Dauchot, and H. Chaté, Collective Motion of Vibrated Polar Disks, Phys. Rev. Lett. **105**, 098001 (2010).

[6] J.-B. Caussin, A. Solon, A. Peshkov, H. Chaté, T. Dauxois, J. Tailleur, V. Vitelli, and D. Bartolo, Emergent Spatial Structures in Flocking Models: A Dynamical System Insight, Phys. Rev. Lett. **112**, 148102 (2014).

[7] I. Theurkauff, C. Cottin-Bizonne, J. Palacci, C. Ybert, and L. Bocquet, Dynamic Clustering in Active Colloidal Suspensions with Chemical Signaling, Phys. Rev. Lett. **108**, 268303 (2012).

[8] M. C. Marchetti, J. F. Joanny, S. Ramaswamy, T. B. Liverpool, J. Prost, M. Rao, and R. A. Simha, Hydrodynamics of soft active matter, Rev. Mod. Phys. **85**, 1143 (2013).

[9] A. Bricard, J.-B. Caussin, N. Desreumaux, O. Dauchot, and D. Bartolo, Emergence of macroscopic directed motion in populations of motile colloids, Nature (London) **503**, 95 (2013).

[10] J. Elgeti, R. G. Winkler, and G. Gompper, Physics of microswimmers—single particle motion and collective behavior: A review, Rep. Prog. Phys. **78**, 056601 (2015).

[11] C. Bechinger, R. Di Leonardo, H. Löwen, C. Reichhardt, G. Volpe, and G. Volpe, Active particles in complex and crowded environments, Rev. Mod. Phys. **88**, 045006 (2016).

[12] A. Baskaran and M. C. Marchetti, Statistical mechanics and hydrodynamics of bacterial suspensions, Proc. Nat. Acad. Sci. USA **106**, 15567 (2009).

[13] J. Toner and Y. Tu, Long-Range Order in a Two-Dimensional Dynamical XY Model: How Birds Fly Together, Phys. Rev. Lett. **75**, 4326 (1995).

[14] T. Vicsek, A. Czirók, El Ben-Jacob, I. Cohen, and O. Shochet, Novel Type of Phase Transition in a System of Self-Driven Particles, Phys. Rev. Lett. **75**, 1226 (1995).

[15] H.-X. Yang, T. Zhou, and L. Huang, Promoting collective motion of self-propelled agents by distance-based influence, Phys. Rev. E **89**, 032813 (2014).

[16] S. Lu, W. Bi, F. Liu, X. Wu, B. Xing, and E. K. L. Yeow, Loss of Collective Motion in Swarming Bacteria Undergoing Stress, Phys. Rev. Lett. **111**, 208101 (2013).

[17] A. Laskar, R. Singh, S. Ghose, G. Jayaraman, P. B. S. Kumar, and R. Adhikari, Hydrodynamic instabilities provide a generic route to spontaneous biomimetic oscillations in chemomechanically active filaments, Sci. Rep. **3**, 1964 (2013).

[18] J. Bialké, T. Speck, and H. Löwen, Crystallization in a Dense Suspension of Self-Propelled Particles, Phys. Rev. Lett. **108**, 168301 (2012).

[19] A. C. H. Tsang and E. Kanso, Circularly confined microswimmers exhibit multiple global patterns, Phys. Rev. E **91**, 043008 (2015).

[20] X. Yang, M. L. Manning, and M. C. Marchetti, Aggregation and segregation of confined active particles, Soft Matter **10**, 6477 (2014).

[21] A. A. Al Sayegh, L. Klushin, and J. Touma, Steady and transient states in low-energy swarms: Stability and first-passage times, Phys. Rev. E **93**, 032602 (2016).

[22] A. P. Solon, H. Chaté, and J. Tailleur, From Phase to Microphase Separation in Flocking Models: The Essential Role of Nonequilibrium Fluctuations, Phys. Rev. Lett. **114**, 068101 (2015).

[23] P. D. Bonkinpillewar, A. Kulkarni, M. V. Panchagnula, and S. Vedantam, A novel coupled fluid-particle DEM for simulating dense granular slurry dynamics, Granular Matter **17**, 511 (2015).

[24] P. S. Mahapatra, S. Mathew, M. V. Panchagnula, and S. Vedantam, Effect of size distribution on mixing of a polydisperse wet granular material in a belt-driven enclosure, Granular Matter **18**, 1 (2016).

[25] D. F. Hinz, A. Panchenko, T.-Y. Kim, and E. Fried, Motility *versus* fluctuations in mixtures of self-motile and passive agents, Soft Matter **10**, 9082 (2014).

[26] C. Drumm, S. Tiwari, J. Kuhnert, and H.-J. Bart, Finite pointset method for simulation of the liquid-liquid flow field in an extractor, Comp. Chem. Eng. **32**, 2946 (2008).

[27] W. C. Swope, H. C. Andersen, P. H. Berens, and K. R. Wilson, A computer simulation method for the calculation of equilibrium constants for the formation of physical clusters of molecules: Application to small water clusters, J. Chem. Phys. **76**, 637 (1982).

[28] S. Plimpton, Fast parallel algorithms for short-range molecular dynamics, J. Comput. Phys. **117**, 1 (1995).

[29] See Supplemental Material at http://link.aps.org/supplemental/10.1103/PhysRevE.95.062610 for thermal motion of the active particles, rotary phase with both single and double vortex, and oscillatory phase.

[30] H. Seyed-Allaei and M. R. Ejtehadi, Vortex with fourfold defect lines in a simple model of self-propelled particles, Phys. Rev. E **93**, 032113 (2016).

[31] H. Wioland, F. G. Woodhouse, J. Dunkel, J. O. Kessler, and R. E. Goldstein, Confinement Stabilizes a Bacterial Suspension into a Spiral Vortex, Phys. Rev. Lett. **110**, 268102 (2013).

[32] T. E. Angelini, E. Hannezo, X. Trepat, M. Marquez, J. J. Fredberg, and D. A. Weitz, Glass-like dynamics of collective cell migration, Proc. Natl. Acad. Sci. USA **108**, 4714 (2011).

[33] S. Henkes, Y. Fily, and M. C. Marchetti, Active jamming: Self-propelled soft particles at high density, Phys. Rev. E **84**, 040301(R) (2011).

[34] L. Berthier and J. Kurchan, Non-equilibrium glass transitions in driven and active matter, Nat. Phys. **9**, 310 (2013).

[35] R. Ni, M. A. C. Stuart, and M. Dijkstra, Pushing the glass transition towards random close packing using self-propelled hard spheres, Nat. Commun. **4**, 2704 (2013).

[36] L. Berthier, Nonequilibrium Glassy Dynamics of Self-Propelled Hard Disks, Phys. Rev. Lett. **112**, 220602 (2014).

[37] Y. Fily, S. Henkes, and M. C. Marchetti, Freezing and phase separation of self-propelled disks, Soft Matter **10**, 2132 (2014).